2018 International Conference on Indoor Positioning and Indoor Navigation (IPIN), 24-27 September 2018, Nantes, France

Error Analysis of ZUPT-Aided Pedestrian Inertial Navigation

Yusheng Wang[1], Andrei Chernyshoff[2], and Andrei M. Shkel[1]
[1]Department of Mechanical and Aerospace Engineering, University of California, Irvine, CA, USA
Email: {yushengw, andrei.shkel}@uci.edu
[2]Independent consultant, Irvine, CA, USA
Email: andrei.chernyshoff@gmail.com

***Abstract*—We present, for the first time, an analytical relation between the navigation errors during Zero-Velocity-Update (ZUPT) aided pedestrian inertial navigation and Inertial Measurement Unit (IMU) performances. Angle Random Walk of gyroscopes and Velocity Random Walk of accelerometers in IMU, velocity measurement uncertainty during the stance phase, and the sampling frequency of IMU are studied and their effects on the overall navigation accuracy are analyzed. Numerical simulation of the ZUPT-aided navigation algorithm is conducted based on a generated pedestrian trajectory to verify the analytical results with the discrepancy less than 30%, showing fidelity of the results. In this study, a foot motion model was developed according to the ambulatory gait analysis as a basis of the numerical simulation. This study may serve as a benchmark for analysis of errors in pedestrian inertial navigation.**

***Index Terms*—Pedestrian navigation, ZUPT, Human gait model, Kalman filter, navigation error**

I. Introduction

The rapid development of micro-electromechanical system (MEMS) based Inertial Measurement Units (IMUs) have made pedestrian navigation possible for positioning in environments where Global Navigation Satellite System (GNSS) is unavailable [1]. This approach is called pedestrian dead-reckoning since it does not depend on pre-installed infrastructure, such as GPS, LTE, and WiFi signals [2]. The relation between the IMU performances and the accumulated navigation errors has also been widely studied and used as a guideline to improve navigation accuracy by reducing IMU errors [3]. Unfortunately, low-cost IMUs still suffer from high noise level and short-term stability, and these errors accumulate during the inertial navigation process. Without an error-suppressing algorithm, the position error accumulates approximately proportional to time cubed and will exceed a meter of error within a few seconds of navigation for consumer grade IMUs [4].

A widely used technique to suppress these errors in pedestrian navigation is the Zero-Velocity-Update (ZUPT) algorithm [5], [6]. During the stance phase of pedestrian walking cycles, the foot periodically returns to a stationary state (zero velocity) when it touches the ground. The ZUPT algorithm takes advantage of this fact and uses the zero-velocity information during the stance phase as a pseudo-measurement fed into the Kalman Filter (KF) to compensate for IMU biases and reduce the navigation error growth in the system. It has been demonstrated that the ZUPT algorithm suppresses the cubic-in-time navigation error growth into growth of a lower order, and renders foot-mounted pedestrian navigation a great potential for practical use [7], [8].

Many numerical and experimental works have been conducted based on ZUPT algorithm to further improve pedestrian navigation accuracy. Complementary measurements, such as magnetometers [9], vision sensors [10], pressure sensors [4], barometers [11], ultrasonic ranging sensors [12], and Radio-Frequency IDentification (RFID) sensors [13], have been proposed and experimentally demonstrated to achieve the goal. However, to the best of our knowledge, no analytical work has been conducted to study the navigation performance in the ZUPT algorithm and to relate the IMU performances to navigation accuracy. This paper intends to fill the gap.

A human gait model is necessary in this study to generate a foot trajectory as a basis for the following numerical simulation study. Although such models have been widely used for bio-mechanical and pathological studies [14], [15], the focus of most approaches are on the extraction of spatial and temporal gait parameters instead of the accumulated motion of the foot over several steps [16]. In this study, a foot motion trajectory is generated through the interpolation and parameterization of previously developed human gait models.

The paper is organized as follows. In Section II, we first generate a foot trajectory based on the human gait model. This will be followed by the analytical study of navigation errors in the ZUPT-aided pedestrian navigation algorithm in Section III. A brief introduction of the algorithm is presented in Section III-A. In Section III-B, a detailed error analysis is discussed and dependence of velocity and angle estimation errors on parameters of IMU and the algorithm is derived. The analytical result is verified by numerical simulations, and major factors affecting the navigation errors are identified in

This work was performed under the following financial assistance award: 70NANB17H192 from U.S. Department of Commerce, National Institute of Standards and Technology (NIST).

Section IV. The paper concludes with a discussion of results in Section V.

II. Foot Trajectory Generation

In this section, we develop an approach for generation of the foot trajectory. Such models are necessary for analytical prediction of errors in ZUPT-aided pedestrian navigation.

Human ambulatory gait models are multi-dimensional due to the complex kinematic and dynamic relations between many parts of human body involved during walking. In this study, our focus is only on the trajectories of two feet instead of the whole-body motion. Therefore, a few assumptions are used to simplify the human gait model:

1) The motion of each leg is two-dimensional and parallel to each other, indicating no rotation occurs at the pelvis and no horizontal rotation occurs at the ankles;
2) The dimensions of both legs are identical;
3) The pattern and duration of each step are identical;
4) The floor is flat, resulting in no accumulation of altitude changes during walking;
5) The trajectory is straight; no turning or stopping happens during the navigation.

In the following parts of this section, we first extract the foot motion from the joints rotation in the torso coordinate frame. Next, based on the human gait analysis, the description of the foot motion is transferred from the torso frame to the navigation frame. Finally, a parameterization is applied to generate a new trajectory with higher order of continuity and while preserving all the key characteristics of the foot motion.

A. Foot Motion in Torso Frame

The torso frame is a coordinate frame that is fixed to the body trunk. In the torso frame, only the relative motion with respect to the trunk is studied.

Joint movement has been widely studied for pathological purposes and the angle data are typically extracted by a high-speed camera or wearable sensors [17]. A pattern of joint angle changes has been reported in [18] and is reproduced in Fig. 1(a). A simplified human leg model is shown in Fig. 1(b). The leg is modeled as two bars with femur length of 50 cm and tibia length of 45 cm. The foot is modeled as a triangle with the side lengths of 4 cm, 13 cm, and 16 cm, respectively. Position of the forefoot in the torso frame is expressed as:

$$x_{forefoot} = L_1 \sin\alpha + L_2 \sin(\alpha-\beta) + L_3 \sin(\alpha-\beta+\gamma), \quad (1)$$

$$y_{forefoot} = L_1 \cos\alpha + L_2 \cos(\alpha-\beta) + L_3 \cos(\alpha-\beta+\gamma). \quad (2)$$

The corresponding parameters are shown in Fig 1(b). The position of another foot can be calculated by shifting the time by half of a cycle since we assume that every step is identical.

B. Foot Motion in Navigation Frame

The navigation frame is the coordinate frame that is fixed on the ground with axes pointing to the north, east, and down directions, respectively. In this frame, the motion of foot with respect to the ground is studied.

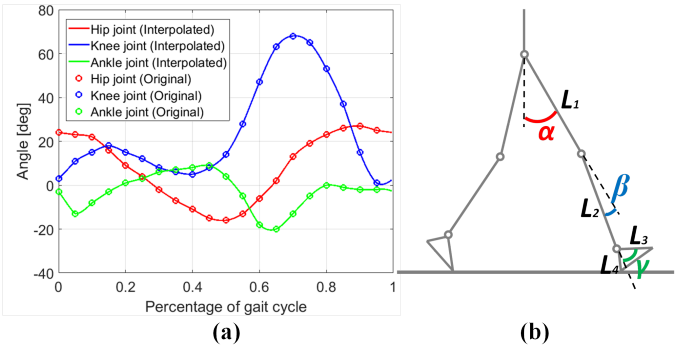

Fig. 1. (a) Interpolation of joint movement data (left) and (b) simplified human leg model (right).

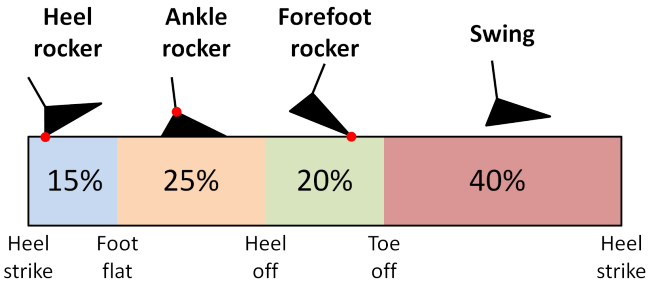

Fig. 2. Human ambulatory gait analysis. Red dots are the stationary points in different phases of one gait cycle.

To transfer a foot motion from the torso frame to the navigation frame, the gait analysis is necessary to establish stationary points as a reference in different phases of the gait cycle. Each gait cycle is divided in two phases: stance and swing. The stance phase is a period during which the foot is on the ground. The swing phase is a period when the foot is in the air for the limb advancement [19].

We assume that each gait cycle begins when the left heel contacts the ground (heel strike). During the first 15% of the gait cycle, the left heel is assumed to be stationary and the foot rotates around it (heel rocker) until the whole foot touches the ground. During 15% to 40% of the gait cycle, the whole left foot is on the ground and stationary, and the left ankle joint rotates for limb advancement (ankle rocker). This is also the time period when zero-velocity update is applied as pseudo-measurements to KF. For 40% to 60% of the gait cycle, the left heel begins to rise and this stage ends when the left foot is off the ground. In this stage, the left foot rotates with respect to the forefoot, which we assume to be stationary (forefoot rocker) [20]. The following part of the gait cycle is symmetric to the previous part since we assume that every step is identical. Phases of the gait cycle are presented in Fig. 2.

After establishing different stationary points in different phases of the gait cycle, we can extract position of the body trunk with respect to the ground. The foot motion can be superimposed on top of the torso motion to obtain the foot motion in the navigation frame.

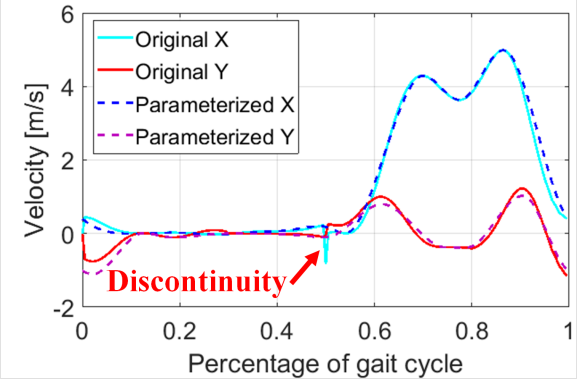

Fig. 3. Velocity of the parameterized trajectory. A close match is demonstrated and discontinuities are eliminated.

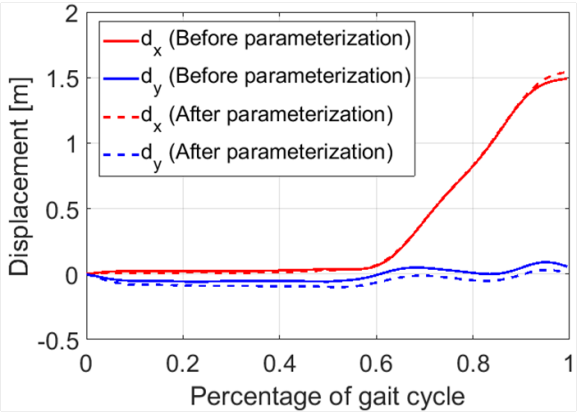

Fig. 4. Displacement of the parameterized trajectory. A close match is demonstrated for displacement along the x direction (horizontal). Difference between the displacements along y direction (vertical) is to guarantee the displacement continuity in between gait cycles.

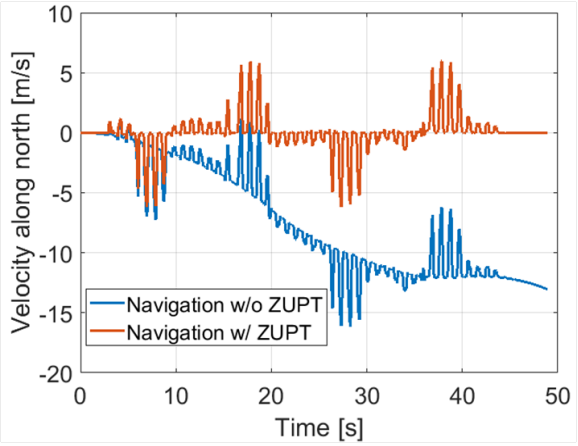

Fig. 5. The comparison between the velocity estimations with and without ZUPT algorithm. The changes in sign correspond to the changes of the direction.

C. Parameterization of Trajectory

Abrupt changes of the reference point from the heel to the ankle and to the forefoot will create discontinuity in the trajectory, especially in terms of velocity and acceleration, as depicted in Fig. 3. The discontinuities of acceleration result in discontinuous accelerometer readouts, which will cause numerical problems in the algorithm. Therefore, parameterization is needed to generate a new trajectory with a higher order of continuity.

The new trajectory to be generated does not have to strictly follow the angle data for each joint and the linkage relations, but ambulatory characteristics should be preserved, especially zero velocity and angular rate during time period of the ankle rocker.

The velocity along the trajectory is parameterized to guarantee the continuity of both displacement and acceleration. Key points are first selected to characterize the IMU velocity along the horizontal and vertical directions. For parameterization along the vertical direction, the integral of velocity for a gait cycle should be zero to make sure the altitude doesn't change over one gait cycle. This is achieved by adjusting velocity values at some of the key points.

The parameterization results are shown in Fig. 3. The generated velocities (dashed lines) closely follow the original values without losing any characteristics and also eliminate the discontinuity that happens in the middle (50%) of the gait cycle, corresponding to a shift of the reference point from the left forefoot to the right heel. The trajectory in terms of position is obtained by integrating the velocity and the results are shown in Fig. 4. A close match is demonstrated for displacement along the horizontal direction. For displacement along the vertical direction, the difference is purposefully introduced to guarantee that the altitude of foot does not change after one gait cycle.

III. Analysis of ZUPT Algorithm

The ZUPT algorithm in inertial pedestrian navigation takes advantage of the stance phase in human gait cycle to compensate for the IMU drifts. The effects of the ZUPT algorithm on the navigation are demonstrated in Fig. 5. Due to biases of the IMU, velocity of the foot drifts without use of the ZUPT algorithm, as presented by the blue line. However, the ZUPT algorithm helps to set the velocity of the foot close to zero during the stance phase and greatly reduces the effects of the IMU biases.

In this section, we will first briefly present how the ZUPT algorithm is achieved by implementing Kalman Filter (KF) on a standard strapdown navigation algorithm. Next, an error analysis will be presented to estimate errors in the ZUPT algorithm and their relation to IMU errors and parameters of the algorithm.

A. Strapdown Navigation with Kalman Filter

We implement a standard strapdown inertial navigation system mechanization in the navigation frame. Drift correction is performed by implementing KF operating on the error states $\delta \boldsymbol{x} = [\delta \boldsymbol{\theta}^T, \delta \boldsymbol{v}_n^T, \delta \boldsymbol{s}_n^T]^T$, where $\delta \boldsymbol{\theta}$ is the attitude error, $\delta \boldsymbol{v}_n$ and $\delta \boldsymbol{s}_n$ are the velocity and position errors along the north, east, and down directions of the navigation coordinate frame

[3]. After each estimation cycle, KF would transfer the error estimation to the INS for the system state compensation. The dynamic error model of KF in this work is approximated by (3):

$$\dot{\delta \boldsymbol{x}} = \begin{bmatrix} 0 & 0 & 0 \\ [\vec{f}^n\times] & 0 & 0 \\ 0 & \boldsymbol{I} & 0 \end{bmatrix} \delta \boldsymbol{x} + \begin{bmatrix} C_b^n \cdot ARW \\ C_b^n \cdot VRW \\ 0 \end{bmatrix} \triangleq A\delta \boldsymbol{x} + B, \quad (3)$$

where $[\vec{f}^n\times]$ is the skew-symmetric cross-product-operator of the accelerometer output in the navigation frame, ARW is Angle Random Walk of the gyroscopes, VRW is the Velocity Random Walk of the accelerometers, and C_b^n is the Directional Cosine Matrix (DCM) from the navigation frame to the body frame. IMU biases are neglected in the model since they are deterministic and can be compensated during the sensor calibration procedure. Scale factor and alignment errors of the IMU are also neglected since they can be eliminated during calibration.

For each time step, besides calculating the system states (position, velocity, and attitude) in the standard strapdown navigation algorithm, we also propagate the priori covariance using

$$P_{k+1|k} = F_k P_{k|k} F_k^T + Q_k, \quad (4)$$

where $P_{k+1|k}$ is defined as the estimation error covariance matrix at $(k+1)^{th}$ time step based on measurements through the k^{th} time step, and F and Q are defined as:

$$F = exp\{A \cdot \Delta t\} \approx I + A \cdot \Delta t,$$
$$Q = diag(B) \cdot \Delta t,$$

where Δt is the time duration of each step. In the discrete form, the system state update can be expressed as

$$\delta \boldsymbol{x}_{k+1|k} = F_k \cdot \delta \boldsymbol{x}_{k|k} + B_k \cdot \Delta t, \quad (5)$$

where $\delta \boldsymbol{x}_{k|k}$ is the estimation of system state from the previous time step (k^{th} step), and $\delta \boldsymbol{x}_{k+1|k}$ is the estimation of system state at the current step without the current measurement inputs.

To activate KF and turn on the ZUPT algorithm, a zero-velocity detector is needed to detect the stance phase in each gait cycle. Generalized Likelihood Rate Test (GLRT) is applied for the zero-velocity detection [16]. In this method, both the variances of acceleration and angular rate are taken into consideration and compared with the threshold set according to the IMU performances. Stance phase is detected and the ZUPT algorithm is turned on if the variance is lower than the threshold value:

$$\text{ZUPT} = H\{\frac{VAR_a}{\sigma_a} + \frac{VAR_g}{\sigma_g} - T\}$$

where $H\{\cdot\}$ is the Heaviside step function, VAR_a and VAR_g are the variances of accelerometer and gyroscope readouts, respectively, σ_a and σ_g are the parameters related to VRW and ARW, respectively, and T is the threshold used in the detector. A demonstration of the detector is shown in Fig. 6.

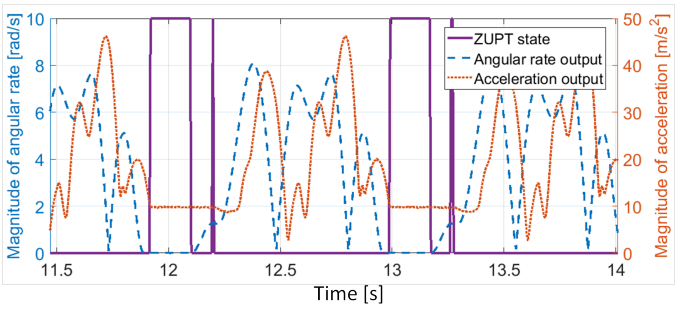

Fig. 6. Demonstration of the implemented zero-velocity detector. The value of ZUPT state (purple line) is either 1 or 0. ZUPT state of value 1 (higher level) indicates the stance phase.

When the stance phase is detected and the ZUPT algorithm is turned on, zero-velocity update is applied as pseudo-measurements and the velocity in the system state is considered as the measurement residual $\boldsymbol{v}_k$ to update the state estimation:

$$\boldsymbol{v}_k = \begin{bmatrix} 0 & I_{3\times 3} & 0 \end{bmatrix} \cdot d\boldsymbol{x}_k + \boldsymbol{w}_k \triangleq H \cdot d\boldsymbol{x}_k + \boldsymbol{w}_k,$$

where H is called the observation matrix, and $\boldsymbol{w}_k$ is the measurement uncertainty, which is the result of two factors: (1) velocity estimation error accumulated during the stance phase, (2) non-zero velocity of the IMU during the stance phase. It has been pointed out that the second factor is a dominant one [21], and the velocity uncertainty value is generally set in the range from 0.001 m/s to 0.1 m/s [5], [21], [22]. The covariance of $\boldsymbol{w}_k$ is denoted by $R_k = E[\boldsymbol{w}_k \boldsymbol{w}_k^T]$.

After KF receives the measurement information, it updates the system state with

$$\delta \boldsymbol{x}_{k+1|k+1} = \delta \boldsymbol{x}_{k+1|k} + K_{k+1} \cdot \boldsymbol{v}_{k+1}, \quad (6)$$

where $\delta \boldsymbol{x}_{k+1|k}$ is an estimation of the system state at the current step with the current measurement inputs $\boldsymbol{v}_{k+1}$, K_k is called the KF gain and it is calculated as

$$K_{k+1} = P_{k+1|k} H_{k+1}^T (H_{k+1} P_{k+1|k} H_{k+1}^T + R_{k+1})^{-1}, \quad (7)$$

and the updated posteriori covariance matrix is

$$P_{k+1|k+1} = (I - K_{k+1} H_{k+1}) P_{k+1|k}. \quad (8)$$

This completes the iteration of the current time step.

B. Navigation Errors Analysis

The ZUPT algorithm is able to reduce the navigation error by restricting the errors in the angle and velocity estimations. Therefore, the quantitative error analysis of the angle and velocity estimations is sufficient in order to analyze the navigation errors in terms of position.

A typical propagation of the error in velocity estimation and its covariance is presented in Fig. 7. The red lines are the actual errors along the north, east, and down directions, respectively. The blue lines are the 3σ limit of the errors. A similar phenomenon can be observed for the angle error

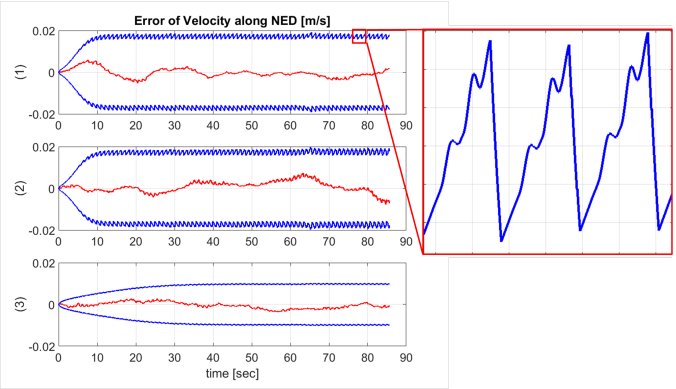

Fig. 7. A typical propagation of errors in velocity estimations in the ZUPT algorithm. (1), (2), and (3) are the velocity along the north, east, and down directions, respectively.

propagations as well. A few conclusions can be drawn from the propagation of errors in velocity estimation:

1) Although the propagation of the errors is random, the covariance propagation follows a pattern;
2) Covariance of the error in velocity estimation reaches a constant level with some fluctuations for all three directions: north, east, and down;
3) The covariances along horizontal directions (north and east) are on the same level, but the covariance along the vertical direction is different;
4) The covariances are reduced when ZUPT is turned on during the stance phase, and they are increased when ZUPT is turned off during the swing phase.

A starting point of the analysis is an observation that the covariances of velocity and angle reach a stable level in the long run of the ZUPT algorithm. This observation indicates that the amount of the covariance increase when the ZUPT is turned off is equal to the amount of the covariance decrease when the ZUPT is turned on. In this way, we combine the ZUPT algorithm parameters that determine ZUPT performances when the ZUPT is turned on and the IMU parameters that dominate in the free navigation when the ZUPT is turned off. The combination enables us to fully analyze the system behavior and extract the covariance of the error in the system state estimation.

1) Covariance increases during walking: Covariance matrix always propagates according to (4), no matter ZUPT is turned on or off, which describes a standard strapdown inertial navigation algorithm. Re-writing (4) into 3×3 sub-blocks and expanding the expression for the sub-block corresponding to the attitude yields:

$$P_{11}^{priori} = P_{11} + Q_{11} \tag{9}$$

In (9), we suppress subscripts indicating the time steps for simplicity, and the new subscripts indicate the index of sub-blocks. The total covariance propagation for the entire swing phase can be estimated by iterating (9). To summarize, the total covariance increase in a complete gait cycle can be approximated as

$$P_{11}^{priori} \approx P_{11} + Q_{11} \cdot N_{stride},$$

where N_{stride} is the number of time steps in one gait cycle. Since the covariance propagations of the two horizontal directions are identical, we only have to focus on one of them. In this study, we only focus on $P_{11}(1,1)$, which corresponds to rotation along the north direction:

$$P_{11}^{priori}(1,1) \approx P_{11}(1,1) + ARW^2 \cdot t_{stride}, \tag{10}$$

where t_{stride} is the time duration of a gait cycle.

Covariance propagation of the velocity estimation error can be analyzed in a similar way based on (4):

$$P_{22}^{priori} \approx P_{22} + Q_{22} + \{[\vec{f}^n\times]P_{12} + P_{21}[\vec{f}^n\times]^T\}\Delta t. \tag{11}$$

$[\vec{f}^n\times]$ is composed of two parts: the acceleration caused by motion and the acceleration caused by gravity. To approximate the term $[\vec{f}^n\times]$, we can separate the two parts and neglect the first part, since the velocity returns to the original value in a complete gait cycle, indicating that integral of the acceleration equals zero. Therefore, the total covariance increase of the velocity error along the north can be expressed as

$$P_{22}^{priori}(1,1) \approx P_{22}(1,1) + (VRW^2 + 2g \cdot P_{12}(1,2)) \cdot t_{stride}, \tag{12}$$

where $P_{12}(1,2)$ is the covariance between the rotation along the north and the velocity along the east, and g is the gravitational acceleration. The reason why $P_{12}(1,2)$ is important is that it corresponds to the coupling between the angular rate error and the velocity error. To complete the analysis, we also need to calculate the covariance increase of $P_{12}(1,2)$:

$$P_{12}^{priori}(1,2) \approx P_{12}(1,2) + g \cdot P_{11}(1,1) \cdot t_{stride}. \tag{13}$$

2) Covariance decrease during the stance phase: ZUPT algorithm is turned on to compensate for the IMU errors during the stance phase and the covariances of the angle and velocity estimations are also reduced. The amount of the total reduction can be calculated based on (7) and (8).

We first analyze the covariance of the angle estimation. For each time step during the stance phase, the covariance change can be expressed as:

$$\begin{aligned} P_{11}^{posteriori}(1,1) &= P_{11}(1,1) - \frac{P_{12}(1,1)P_{21}(1,1)}{P_{22}(1,1)+R(1,1)} \\ &\quad - \frac{P_{12}(1,2)P_{21}(2,1)}{P_{22}(2,2)+R(2,2)} - \frac{P_{12}(1,3)P_{21}(3,1)}{P_{22}(3,3)+R(3,3)} \\ &\approx P_{11}(1,1) - \frac{P_{12}(1,2)^2}{R(2,2)}. \end{aligned} \tag{14}$$

In the strapdown inertial navigation mechanization, the rotation along the north is strongly coupled with the acceleration along the east due to the gravity. Therefore, $P_{12}(1,1)$ and $P_{12}(1,3)$ are much smaller than $P_{12}(1,2)$ and can be neglected. The velocity measurement uncertainty is generally much greater than velocity error induced by IMU errors in

the ZUPT algorithms. As a result, $P_{22}(2,2)$ is smaller than $R(2,2)$ and can be neglected.

Similarly, changes in covariance of the coupling term $P_{12}(1,2)$ and the velocity term $P_{22}(2,2)$ in one time step can be also calculated:

$$P_{12}^{posteriori}(1,2) \approx P_{12}(1,2) - \frac{P_{12}(1,2)P_{22}(2,2)}{R(2,2)}, \quad (15)$$

$$P_{22}^{posteriori}(2,2) \approx P_{22}(2,2) - \frac{P_{22}(2,2)^2}{R(2,2)}. \quad (16)$$

3) Covariance level estimation: It has been observed that the covariances remain on a constant level. Therefore, the covariance increase due to the IMU noises should be equal to the covariance drop during the stance phase.

A combination of (10) and (14) gives

$$ARW^2 \cdot t_{stride} = \frac{P_{12}(1,2)^2}{R(2,2)} \cdot N_{stance}, \quad (17)$$

Since $N_{stance} = f_s \cdot t_{stance}$, P_{12} can be expressed as

$$P_{12}(1,2) = ARW[\frac{R(2,2) \cdot t_{stride}}{f_s \cdot t_{stance}}]^{1/2}, \quad (18)$$

where f_s is the sampling frequency of the IMU. Similarly, the combination of (12) and (16) gives us

$$\frac{P_{22}(2,2)^2}{R(2,2)} N_{stance} = (VRW^2 + 2g \cdot P_{12}(1,2)) \cdot t_{stride}, \quad (19)$$

or re-arranging the terms:

$$\begin{aligned} P_{22}(2,2) = [2g \cdot ARW(\frac{R(2,2)t_{stride}}{f_s \cdot t_{stance}})^{3/2} \\ + VRW^2 \frac{R(2,2)t_{stride}}{f_s \cdot t_{stance}}]^{1/2}. \end{aligned} \quad (20)$$

$P_{22}(2,2)$ is the term in the covariance matrix that corresponds to uncertainty of the velocity estimation along the east. The velocity uncertainty is simply $\sigma_v = \sqrt{P_{22}(2,2)}$.

The combination of (13) and (15) gives us

$$\frac{P_{12}(1,2)P_{22}(2,2)}{R(2,2)} N_{stance} = g \cdot P_{11}(1,1) \cdot t_{stride}, \quad (21)$$

and P_{11} can be expressed as

$$\begin{aligned} P_{11}(1,1) = [\frac{2}{g} \cdot ARW^3(\frac{R(2,2)t_{stride}}{f_s \cdot t_{stance}})^{1/2} \\ + (\frac{ARW \cdot VRW}{g})^2]^{1/2}. \end{aligned} \quad (22)$$

The uncertainty of the angle estimation along the north is $\sigma_\theta = \sqrt{P_{11}(1,1)}$.

To summarize, the relations between the IMU errors and the navigation errors in terms of velocity and angle uncertainties are derived and explicitly represented as follows:

$$\sigma_v = [2gARW(\frac{R(2,2)t_{stride}}{f_s \cdot t_{stance}})^{3/2} + VRW^2 \frac{R(2,2)t_{stride}}{f_s \cdot t_{stance}}]^{1/4}, \quad (23)$$

$$\sigma_\theta = [\frac{2}{g} ARW^3(\frac{R(2,2)t_{stride}}{f_s \cdot t_{stance}})^{1/2} + (\frac{ARW \cdot VRW}{g})^2]^{1/4}. \quad (24)$$

4) Observations:

1) ARW and VRW are coupled and they both have influence on the final angle and velocity uncertainties; higher ARW and VRW result in larger navigation errors;
2) The velocity measurement uncertainty $R(2,2)$ plays an important role in the final results; lower $R(2,2)$ indicates a higher reliability and weight of the zero-update information in KF, resulting in a better navigation accuracy;
3) The ratio between duration of the stance phase and the whole gait cycle also affects the navigation errors. Higher percentage of the stance phase during the gait cycle gives KF more data to compensate for the IMU errors and reduce the overall navigation errors;
4) Higher sampling frequency f_s enables the system to provide more measurements to KF during the stance phase and thus helps to reduce the navigation errors in the ZUPT algorithm;
5) Equation (23) and (24) are only the approximations of the navigation errors due to assumptions and approximations made during the derivation; validity of the approximations will be demonstrated in the following section.

IV. Numerical Analysis

In this section, we apply the ZUPT algorithm on the trajectory generated based on results discussed in Section II. Then, the numerical results are compared to the analytical expressions in (23) and (24). The generated trajectory is a straight line toward north containing 100 steps. The total time duration of the trajectory is 53.6 s and the total length of the trajectory is 77 m.

A. Effects of ARW

We first study the influence of the ARW of IMU gyroscopes on the navigation errors. We sweep the ARW value from 0.01 $deg/\sqrt{hr}$ to 10 $deg/\sqrt{hr}$ (from near navigation grade to consumer grade), while keeping other parameters constant: VRW of accelerometers is set to be 0.14 $mg/\sqrt{Hz}$ (tactical grade), the velocity measurement uncertainty is set to be 0.01 m/s, and the sampling frequency is 200 Hz. The simulation results are presented in Fig. 8. The upper plot shows the relation between the ARW and the velocity estimation uncertainty and the lower plot shows the relation between the ARW and the angle estimation uncertainty. In both plots, the blue lines are the results derived from (23) and (24), and the red error bars are from the simulation results. The reason why simulation results are a range instead of a value is that the covariances of the estimation errors fluctuate during the navigation (see Fig. 7). The upper and lower bounds of the error bars show the amplitude of fluctuation and the square shows an average value of the fluctuation.

A close match between the two results verifies validity of the analysis. Fig. 8 shows that the velocity estimation uncertainty is not affected by ARW when it is smaller than 0.1 $deg/\sqrt{hr}$ and the lower bound of the fluctuation is not

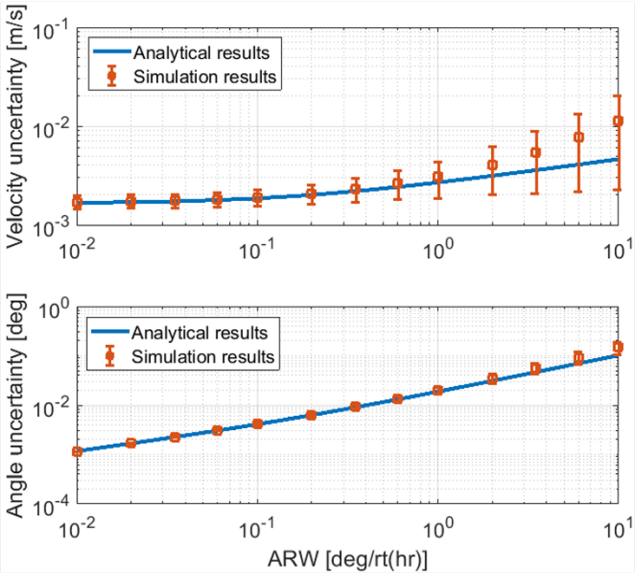

Fig. 8. Effects of ARW of the IMU gyroscopes on the navigation errors in ZUPT algorithm.

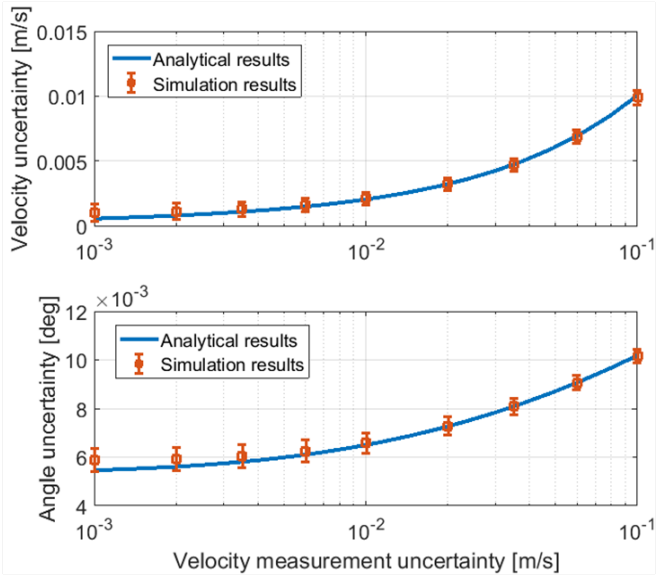

Fig. 10. Effects of velocity measurement uncertainty during the stance phase on navigation errors in the ZUPT algorithm.

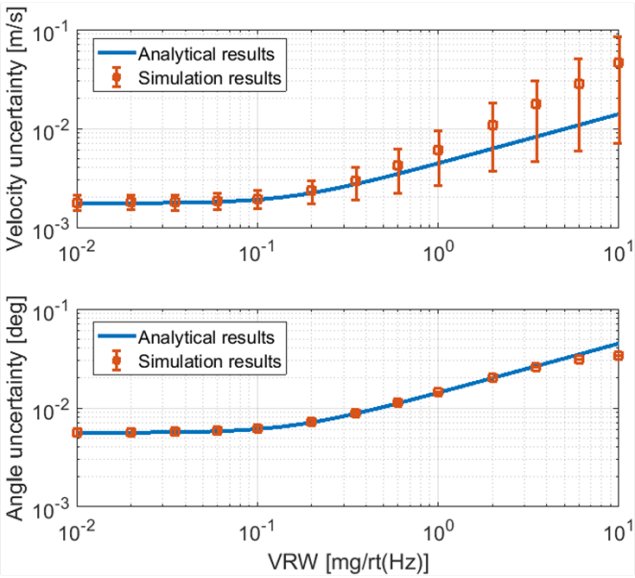

Fig. 9. Effects of VRW of the IMU on the navigation errors in ZUPT algorithm.

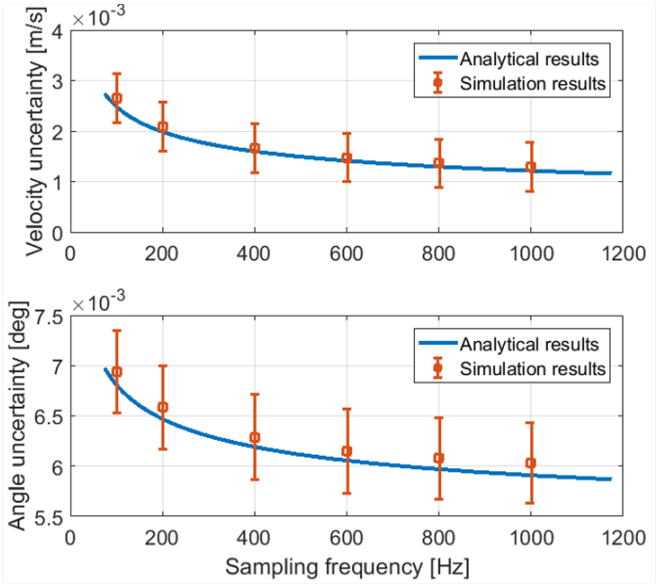

Fig. 11. Effects of the sampling rate of IMU on navigation errors in the ZUPT algorithm.

affected by it either. This is because the lower bound of the velocity uncertainty is limited by the velocity measurement uncertainty set in KF, which is fixed in this model. As for the independence of the average value when ARW is small, one possible reason is that the performance of accelerometers is worse than that of the gyroscopes in this case, and the velocity uncertainty is dominated by the accelerometer errors, therefore is independent of gyroscope errors. However, the angle estimation uncertainty is still affected by ARW even when it is small, indicating that the gyroscope error is a dominant source for the angle estimation errors even when gyroscopes are much better than accelerometers in IMUs. It is also noticed that fluctuation of the angle uncertainty is much smaller than the velocity uncertainty. The reason is that the velocity is directly observable in the ZUPT algorithm, and therefore, KF can directly estimate the optimal velocity value and reduce the velocity uncertainty. The angle estimation, however, is achieved through coupling the velocity and angle, and subsequently the observability is reduced.

B. *Effects of VRW*

Similarly, we sweep the VRW value of accelerometers from 0.01 $mg/\sqrt{Hz}$ to 10 $mg/\sqrt{Hz}$ while keeping ARW of the gyroscope to be 0.21 $deg/\sqrt{hr}$ (tactical grade). The results

are shown in Fig. 9. As expected, the curves become flat when VRW is small, since the navigation error is dominated by gyroscope errors in this range.

C. Effects of Velocity Measurement Uncertainty

To understand the effect, we sweep the velocity measurement uncertainty during the stance phase from 0.001 m/s to 0.1 m/s and keep the ARW of gyroscopes to be 0.21 $deg/\sqrt{hr}$ and VRW of accelerometers to be 0.14 $mg/\sqrt{Hz}$. The results are shown in Fig. 10. The results show that the navigation error is different even with the same IMU performance and trajectory. As a result, a lower velocity measurement uncertainty is desirable for a better navigation accuracy. The following considerations can help to reduce the velocity measurement uncertainty and improve the overall navigation accuracy: (1) a stiffer shoe with less deformation during walking, (2) a better position to attach the IMU so that IMU can be truly stationary during the stance phase, and (3) shock absorber on the shoes to prevent strong shocks between the shoe and the ground.

D. Effects of Sampling Frequency of IMU

A higher sampling frequency of the IMU gives KF more measurements for the system state corrections, since higher sampling frequency indicates more time steps during the stance phase, and it therefore helps to reduce the navigation errors. A 2.5$\times$ drop of velocity uncertainty has been demonstrated by increasing the sampling rate from 100 Hz to 1000 Hz in Fig. 11.

V. Conclusions

In this paper, for the first time, we presented an analytical relation between the navigation errors during ZUPT-aided pedestrian inertial navigation and IMU performances. The effects of ARW of the gyroscopes and VRW of the accelerometers in IMU, velocity measurement uncertainty during the stance phase, and sampling frequency on the navigation error are analytically derived and numerically confirmed.

Foot motion trajectory was generated through the interpolation and parameterization of human ambulatory gait model. It serves as a basis for the presented numerical simulation of the ZUPT-aided pedestrian inertial navigation.

This study is envisioned to aid in analysis of the effect of errors in sensors, which might lead to a well informed selection of sensors for the task of ZUPT-aided pedestrian inertial navigation.

Acknowledgment

All the analytical and numerical work was conducted in the MicroSystems Laboratory of the University of California, Irvine.

References

[1] X. Yun, E. R. Bachmann, H. Moore, and J. Calusdian, "Self-contained position tracking of human movement using small inertial/magnetic sensor modules." 2007 IEEE International Conference on Robotics and Automation, Apr. 10-14, 2007, Roma, Italy, pp. 2526-2533.

[2] A. R. Jimenez, F. Seco, C. Prieto, and J. Guevara, "A comparison of pedestrian dead-reckoning algorithms using a low-cost MEMS IMU." IEEE International Symposium on Intelligent Signal Processing, 2009. Aug. 26-28, 2009, Budapest, Hungary, pp. 37-42.

[3] D. Titterton and J. Weston, Strapdown inertial navigation technology, 2nd ed., vol. 207. AIAA, 2004, pp. 30.

[4] M. Ma, Q. Song, Y. Li, and Z. Zhou, "A zero velocity intervals detection algorithm based on sensor fusion for indoor pedestrian navigation." 2017 IEEE 2nd Information Technology, Networking, Electronic and Automation Control Conference (ITNEC), Dec. 15-17, 2017, Chengdu, China, pp. 418-423.

[5] E. Foxlin, "Pedestrian tracking with shoe-mounted inertial sensors." IEEE Computer graphics and applications, vol. 25, no. 6, pp. 38-46, 2005.

[6] J. O. Nilsson, A. K. Gupta, and P. Handel, "Foot-mounted inertial navigation made easy." 2014 International Conference on Indoor Positioning and Indoor Navigation (IPIN), Oct. 27-30, 2014, Busan, Korea, pp. 24-29.

[7] S. Godha, and G. Lachapelle, "Foot mounted inertial system for pedestrian navigation." Measurement Science and Technology, vol. 19, no. 7, pp. 075202, 2008.

[8] C. Tjhai, and K. O'Keefe, "Step-size estimation using fusion of multiple wearable inertial Sensors." 2017 International Conference on Indoor Positioning and Indoor Navigation (IPIN), Sep. 18-21, 2017, Sapporo, Japan, pp. 18-21.

[9] H. Hellmers, A. Norrdine, J. Blankenbach, and A. Eichhorn, "An IMU/magnetometer-based indoor positioning system using Kalman filtering." 2013 International Conference on Indoor Positioning and Indoor Navigation (IPIN), Oct. 28-31, 2013, Montbeliard-Belfort, France, pp. 1-9.

[10] Y. Zhang, J. Tan, Z. Zeng, W. Liang, and Y. Xia, "Monocular camera and IMU integration for indoor position estimation." 2014 36th IEEE Annual International Conference, Engineering in Medicine and Biology Society (EMBC), Aug. 26-30, 2014, Chicago, IL, USA, pp. 1198-1201.

[11] A. Norrdine, Z. Kasmi, and J. Blankenbach, "Step detection for ZUPT-aided inertial pedestrian navigation system using foot-mounted permanent magnet." IEEE Sensors Journal, vol. 16, no. 17, pp. 6766-6773, 2016.

[12] F. Olsson, J. Rantakokko, and J. Nygrds, "Cooperative localization using a foot-mounted inertial navigation system and ultrawideband ranging." 2014 International Conference on Indoor Positioning and Indoor Navigation (IPIN), Oct. 27-30, 2014, Busan, Korea, pp. 122-131.

[13] A. D. J. Ruiz, F. S. Granja, J. C. P. Honorato, and J. I. G. Rosas, "Accurate pedestrian indoor navigation by tightly coupling foot-mounted IMU and RFID measurements." IEEE Transactions on Instrumentation and measurement, vol. 61, no. 1, pp. 178-189, 2012.

[14] H. M. Schepers, H. F. Koopman, and P. H. Veltink, "Ambulatory assessment of ankle and foot dynamics." IEEE Transactions on Biomedical Engineering, vol. 54, no. 5, pp. 895-902, 2007.

[15] S. J. M. Bamberg, A. Y. Benbasat, D. M. Scarborough, D. E. Krebs, and J. A. Paradiso, "Gait analysis using a shoe-integrated wireless sensor system." IEEE Transactions on Information Technology in Biomedicine, vol. 12, no. 4, pp. 413-423, 2008.

[16] I. Skog, P. Handel, J. O. Nilsson, and J. Rantakokko, "Zero-velocity detection—-An algorithm evaluation." IEEE Transactions on Biomedical Engineering, vol. 57, no. 11, pp. 2657-2666, 2010.

[17] W. Tao, T. Liu, R. Zheng, and H. Feng, "Gait analysis using wearable sensors." Sensors, vol. 12, no. 2, pp. 2255-2283, 2012.

[18] M. P. Murray, A. B. Drought, and R. C. Kory, "Walking gait of normal man." Journal of Bone & Joint Surgery, vol. 46, pp. 335-360, 1964.

[19] J. Perry, and J. R. Davids, "Gait analysis: normal and pathological function." Journal of Pediatric Orthopaedics, vol. 12, no. 6, pp. 815, 1992.

[20] M. W. Whittle, Gait analysis: an introduction, 3rd ed., Oxford: Butterworth-Heinemann, 2002.

[21] M. Ren, K. Pan, Y. Liu, H. Guo, X. Zhang, and P. Wang, "A novel pedestrian navigation algorithm for a foot-mounted inertial-sensor-based system." Sensors, vol. 16, no. 1, pp.139, 2016.

[22] I. Skog, J. O. Nilsson, and P. Handel, "Evaluation of zero-velocity detectors for foot-mounted inertial navigation systems." IEEE 2010 International Conference on In Indoor Positioning and Indoor Navigation (IPIN), Sept 15-17, 2010, Zurich, Switzerland, pp. 1-6.